Proceedings of the ASME 2020
International Design Engineering Technical Conferences
and Computers and Information in Engineering Conference
IDETC/CIE2020
August 17-19, 2020, Virtual, Online

DETC2020-22173

A NEW EXTENSIBLE CONTINUUM MANIPULATOR USING FLEXIBLE PARALLEL MECHANISM AND RIGID MOTION TRANSMISSION

Yujiong Liu, Pinhas Ben-Tzvi*
Robotics and Mechatronics Laboratory
Mechanical Engineering Department
Virginia Tech
Blacksburg, VA, USA

ABSTRACT

An extensible continuum manipulator (ECM) has specific advantages over its non-extensible counterparts. For instance, in certain applications, such as minimally invasive surgery or tube inspection, the base motion might be limited or disallowed. The additional extensibility provides the robot with more dexterous manipulation and larger workspace. Existing continuum robot designs achieve extensibility mainly through artificial muscle/pneumatic, extensible backbone, concentric tube, and base extension etc. This paper proposes a new way to achieve this additional motion degree of freedom by taking advantage of the rigid coupling hybrid mechanism concept and a flexible parallel mechanism. More specifically, a rack and pinion set is used to transmit the motion of the i-th subsegment to drive the (i+1)-th subsegment. A six-chain flexible parallel mechanism is used to generate the desired spatial bending and one extension mobility for each subsegment. This way, the new manipulator is able to achieve tail-like spatial bending and worm-like extension at the same time. A proof-of-concept prototype was integrated to verify the mobility of the new mechanism. Corresponding kinematic analyses are conducted to estimate the workspace and the motion non-uniformity.

1 INTRODUCTION

Inspired by nature, continuum robots, especially continuum manipulators, are developed to achieve animal-like compliant-to-object property. This property is thought critical for certain applications that require passive compliance, for instance, medical robots that need to interact with human tissues, manipulation robots that need to handle fragile objects, or exploration robots that need to go through unexpected narrow passages. Traditional solutions for this kind of robots focus on using deformable materials (e.g., an elastic backbone) and deformable actuation (e.g., tendon or rod driven). Existing examples using this technology include the Elephant trunk [1], Tentacle robot [2], and the DDU [3], etc.

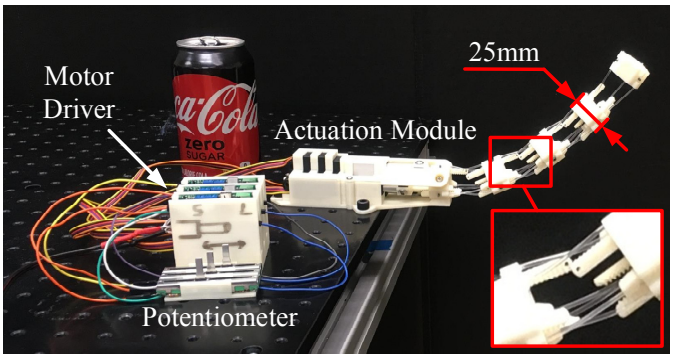

Figure 1. Proof-of-concept prototype of the new extensible continuum manipulator

Another solution is a hyper-redundant structure, which is not theoretically a continuum robot but can behave like one. The proposed design utilizes traditional serially connected rigid link structures and usually distributes/transmits the actuation on each joint. The typical representations for this category are snake-like robots [4-6] and multi-link tail robots [7-9].

Limited by the mechanism structure and the actuation technology, the aforementioned solutions are usually not extensible. However, for certain applications where the manipulator base motion is constricted or disabled, worm-like extensibility can significantly augment the manipulability and dexterity. To add the extension mobility, the easiest way might be to modify the backbone structure of the traditional continuum robots to make them extensible. Some approaches applying this idea include the NASA Tendril [10] which uses extension and compression springs as the backbone, the tendon-driven continuum robot [11] which takes advantage of the magnetic repulsion force for backbone extension, the extensible continuum robot [12] using origami modules, and the concentric tube robot [13]. However, except for the concentric tube robot,

*Corresponding author – bentzvi@vt.edu

the extension motion of most extensible manipulators in this type is usually passive, especially when a tendon driven system is used. This causes the shortcoming that the manipulator stiffness decreases significantly as the manipulator extends. Therefore, besides making the backbone extensible, a more straightforward way is to directly use an extensible actuator, such as a pneumatic actuator or an artificial muscle [14]. This approach avoids the passive extension disadvantage but usually suffers from other shortcoming such as the need to use a heavy actuator and control implementation issues.

Rigid coupling hybrid mechanism (RCHM) is a new family of hybrid mechanisms that was previously proposed by the authors to design multi-link robotic tails [15]. This type of mechanisms take advantage of the traditional hybrid mechanism structure [16] but use specific transmission mechanisms to couple adjacent subsegment mechanisms. Following this novel motion transmission idea, designing curvature bending robots based on rigid links becomes possible and more importantly, designing general manipulation robots with special mobility requirements is also promising since the vast existing parallel mechanisms could be well utilized as subsegment mechanisms.

Therefore, this paper aims to apply the RCHM idea to develop a new type of extensible continuum manipulator (ECM) that has both the advantages of the extensible backbone approach (relatively small actuator) and the extensible actuator approach (active extension control). The desired ECM should have 3DOF in total, in which two achieve the spatial bending mobility and one achieves the axial extension mobility. An overview of the final prototype is shown in Fig. 1.

The following sections are organized as follows. Section 2 introduces the background and motivation in detail. Section 3 describes the mechanical design of the robot system. Section 4 formulates the kinematics based on constant curvature bending assumption and conducts workspace analysis as well as motion non-uniformity evaluation accordingly. Section 5 presents the prototyping details and the experimental results. The conclusion section recaps the main points of this paper and discusses future work.

2 RIGID COUPLING HYBRID MECHANISM

This section presents the previously proposed rigid coupling hybrid mechanism concept, which is the foundation of the new mechanism in this paper.

The RCHM concept was proposed to address the challenge of designing spatial curvature bending mechanisms based on rigid links. The core idea is to take advantage of the motion from the i-th link to drive the (i+1)-th link instead of transmitting motion directly from the base to each link. This method of motion transmission is realized by the "rigid coupling" mechanism that couples the (i+1)-th link with the i-th link. As for the basic mobility for each subsegment, traditional parallel mechanisms are used. Therefore, combining these two mechanism components, the new hybrid mechanism is able to amplify the subsegment mobility to the manipulator scale. For instance, a 3DOF spatial RCHM may be designed by serially connecting 3DOF parallel mechanisms and using rigid transmission mechanisms to couple the adjacent parallel mechanisms.

Figure 2 shows the topological structure of the RCHM, which mainly consists of five components: base, actuation, link, parallel mechanism (PM), and rigid transmission mechanism (RTM). The PMs realize the basic motion for each subsegment. The RTMs serve as the "rigid coupling" mechanisms that transmit motion from the i-th PM to the (i+1)-th PM. Therefore, the overall motion sequence is that the actuators drive PM1 directly, then the RTM1 copies the PM1 motion to drive PM2. After PM2 moves, RTM2 transmits the motion from PM2 to drive PM3, and so on and so forth.

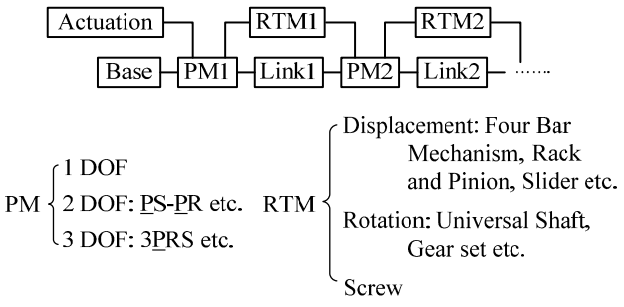

Figure 2. The rigid coupling hybrid mechanism concept

RCHM has two main advantages compared with traditional cable driven hyper-redundant designs. Firstly, RCHM usually has good rigidity due to the parallel mechanism used for each subsegment, which is known to have higher stiffness, precision and load bearing in comparison to its serial counterpart. Moreover, using rigid transmission design avoids the commonly observed cable driven issues, such as the unidirectional driving problem and the cable tension control problem. These two features, together, provide the RCHM with good rigidity and enable the mechanism to respond to high frequency input, which is critical for applications that need high speed or high dynamic motion. Secondly, since the RCHM has centralized actuation, the weight of the robot itself could be significantly reduced. As a result, the motion accuracy of the robot could be increased and the controller could be simplified.

3 MECHANICAL DESIGN

This section details the mechanical design of the new extensible manipulator. For subsequent discussions, "P" stands for prismatic joint, "R" stands for revolute joint, and "S" stands for spherical joint (which is also referred to as ball joint). An actuated joint is labeled by an underlined letter.

3.1 PM Design Using Flexible Parallel Mechanism

The first step for the RCHM design is to select the appropriate PM to realize the subsegment motion, which is the 2R1T (two radial rotations and one axial translation) motion in this case. There are many existing researches on the mechanism synthesis for this motion [17], among which the simplest might

be the 3PSR mechanism [18]. However, to take advantage of the motion generated by this 3PSR mechanism and transmit motion to the next subsegment, another three chains are required. These three additional chains are placed close to the three original chains respectively so that each additional chain behaves simultaneously and similarly with its original chain counterpart. This way, the additional chains are able to "measure" the motion generated by the original chains. Therefore, these three additional chains are usually called "Measuring PM" while the original three chains are called "Driving PM" due to their different functionalities. It is important to note that due to the physical thickness of the links, the closeness of the additional chain with the original chain could never become zero, which leads to the fact that the "Measuring PM" could never exactly copy the motion of the "Driving PM". As a result, this fact brings in non-uniform twist motions (the non-uniformity could be very small if the two chains were designed close enough) among subsegments. More details about this will be discussed in section 4.4.

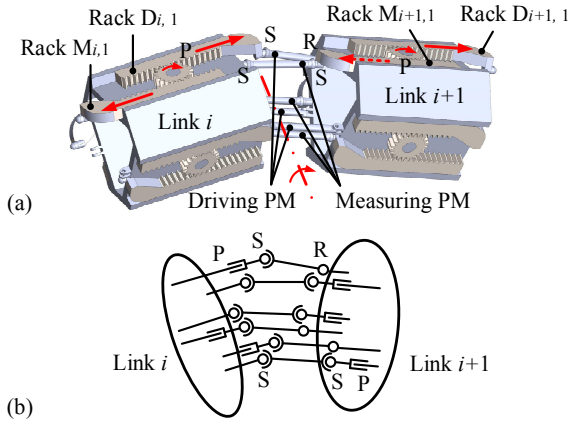

Figure 3. (a) The original PM design using rigid links and rigid joint (b) The corresponding kinematic diagram of the PM

Since the "Driving PM" is already fully constrained, the three additional chains cannot exert more constraints onto the system. Therefore, three SSP chains are selected to guarantee enough degrees of freedom for the "Measuring PM". Fig. 3a shows one potential subsegment design based on this mechanism configuration and Fig. 3b is the corresponding kinematic diagram. The overall mobility can be verified by the Grübler-Kutzbach criterion (G-K criterion) [19] as

$$M = 6n - \sum_{i=1}^{j}(6 - f_i) \tag{1}$$
$$= 6 \times 13 - 3 \times (5 + 3 + 5) - 3 \times (3 + 3 + 5) = 6$$

where n is the number of moving bodies, j is the number of joints, and f_i is the corresponding DOF of joint i. Although the calculation shows the mechanism having 6 DOF, three of them are actually internal DOF (self-rotation with respect to the axis connecting the two ball joint centers) induced by the SS chains, which do not affect the overall mobility. Therefore, the actual mobility of the 3PSR-3SSP mechanism is 3.

The PM together with the rack and pinion transmission forms the basic motion propagation mechanism. For instance, referring to Fig. 3a, if an input motion (indicated by the solid arrow) is exerted on Rack $M_{i,1}$, Rack $D_{i,1}$ is pushed right through the gear. This motion causes the clockwise rotation of Link i+1, which further induces the relative motion of $M_{i+1,1}$ (indicated by the dashed arrow). Because of the gear, this relative motion continues to be transmitted onto Rack $D_{i+1,1}$, which becomes the driving motion for the next subsegment.

Using rigid links and joints provide the advantages of being able to bear larger load and having higher stiffness. The disadvantages include complicated mechanical structure that makes the manufacturing process more challenging in terms of manufacturing tolerance control problems (e.g., backlash is rapidly amplified due to the motion propagation characteristics of this type of mechanism). Therefore, flexible parallel mechanisms [20,21] (FPM) are proposed to replace the rigid link-based PM. The flexible structure facilitates the manufacturing process significantly and increases the accuracy by avoiding backlash (i.e., the deformation of the material itself does not induce backlash). Moreover, the flexible structure has the same compliant-to-obstacle benefit as traditional continuum robots.

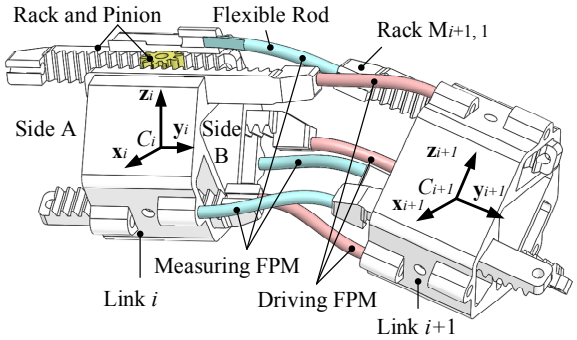

Figure 4. The modified PM design that uses flexible rods to replace the rigid links and rigid joints. A local section view of link *i* shows the internal rack and pinion transmission mechanism.

As show in Fig. 4, the modified subsegment design uses flexible rods to replace the original rigid links and joints. Similarly, the six chain FPM is subdivided to one "Driving FPM" and one "Measuring FPM". After changing to flexible rods, the mounting and connection among parts become easier too. For instance, the rods could be easily connected with the racks and the links using glue. The rack and pinion sets are also placed internally to achieve better assembly accuracy.

3.2 System Assembly

Figure 5 shows the overall design of the new ECM, where

the ECM body is comprised of four serially connected subsegments. Customized housing covers are designed to mount three linear actuators. The connection between the actuation module and the ECM body is achieved by a specifically designed first link and three special racks.

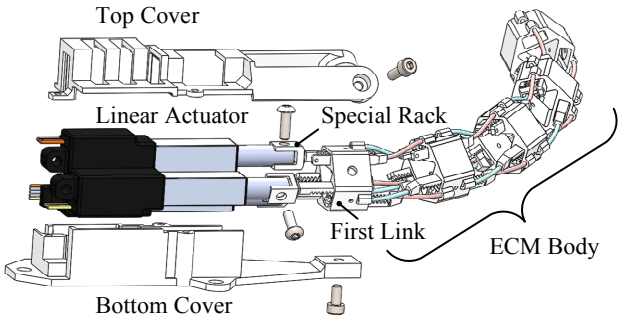

Figure 5. Overall design of the new ECM

4 KINEMATIC ANALYSIS

For the preliminary kinematic analysis, certain assumptions could be made to simplify the computation. Due to similar mobility as the traditional extensible continuum manipulator, circular arc bending [22] is also assumed here. That is, each subsegment is regarded as a constant curvature bending continuum robot section and each rod together with its rack is regarded as the driving cable/rod for that continuum robot section. This way, each subsegment shape is fully defined by the three chains in the "Driving FPM" and the three chains in the "Measuring FPM" only measure the corresponding arc length and transmits to the next subsegment.

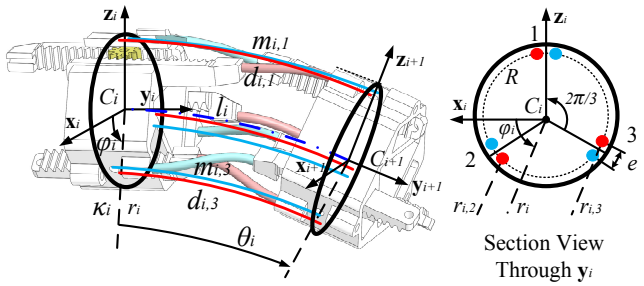

Figure 6. Subsegment kinematic model based on the circular arc bending assumption

4.1 Subsegment Kinematics

Figure 6 illustrates the subsegment kinematic model based on the circular arc bending assumption, where the red arcs are the abstraction of the driving chains with length $d_{i,j}$ and the blue arcs are the abstraction of the measuring chains with length $m_{i,j}$. $i \in \{1,2,3,4\}$ represents the i-th link and $j \in \{1,2,3\}$ represents the j-th chain in one subsegment. Body fixed frame $\sum C_i = (C_i, \mathbf{x}_i, \mathbf{y}_i, \mathbf{z}_i)$ is placed at the center of the i-th link. l_i, κ_i, r_i, and θ_i denote the arc length, curvature, radius, and central angle for the central bending arc (in purple dash-dot line), respectively. φ_i is the angle of the bending plane from $\mathbf{x}_i$ axis, R is the distance of the driving/measuring arcs from the central arc. Based on mathematical definitions, the following relationships are self-satisfied

$$l_i = \theta_i r_i \tag{2}$$

$$r_i = 1/\kappa_i \tag{3}$$

Therefore, with three arc lengths $d_{i,j}$, the bending shape is fully determined. The forward kinematics is obtained in the same way as in [22]

$$l_i = \frac{d_{i,1} + d_{i,2} + d_{i,3}}{3} \tag{4}$$

$$\kappa_i = \frac{2\sqrt{d_{i,1}^2 + d_{i,2}^2 + d_{i,3}^2 - d_{i,1}d_{i,2} - d_{i,1}d_{i,3} - d_{i,2}d_{i,3}}}{R(d_{i,1} + d_{i,2} + d_{i,3})} \tag{5}$$

$$\varphi_i = -\text{atan2}\left(d_{i,3} + d_{i,2} - 2d_{i,1}, \sqrt{3}\left(d_{i,3} - d_{i,2}\right)\right) + \frac{e}{2R} \tag{6}$$

where the second term in Eq. (6) is the angle shift due to the mounting point offset of the driving arc on the sectional view plane (the red dots are not exactly located on the $\mathbf{z}_i$ axis).

Knowing the bending shape, the three measuring arc lengths could be obtained by inverse kinematics as

$$m_{i,j} = l_i - l_i\kappa_i R\cos(\varphi_i + \frac{e}{2R} + \frac{7\pi}{6} - \frac{2\pi}{3}j) \tag{7}$$

For the (i+1)-th subsegment, the driving arc length should be replaced by the measuring arc length from the i-th subsegment. That is

$$d_{i+1,j} = m_{i,j} \tag{8}$$

Note that the above and the following equations do not include the $\kappa_i = 0$ case, which could be easily handled in actual programming by manually assigning values to all the variables.

4.2 Overall Kinematics

The overall kinematic model could be easily obtained as long as the subsegment wise kinematics is known. That is, with l_i, κ_i, and φ_i known, the vector from C_i to C_{i+1} is obtained as

$$\mathbf{p}_{i,i+1} = r_i\sin\theta_i\mathbf{y}_i + (r_i - \cos\theta_i r_i)(\cos\varphi_i\mathbf{x}_i - \sin\varphi_i\mathbf{z}_i) \tag{9}$$

The rotation from $\sum C_i$ to $\sum C_{i+1}$ is formulated as

$${}^i\mathbf{R}_{i+1} = e^{\theta_i\hat{\boldsymbol{\xi}}} \tag{10}$$

where $\boldsymbol{\xi} = -\sin\varphi_i\mathbf{x}_i - \cos\varphi_i\mathbf{z}_i$ is the rotation axis vector and the hat above $\boldsymbol{\xi}$ indicates the skew-symmetric expansion. Equation (10) could be easily evaluated by the Rodrigues' formula [23] as

$${}^i\mathbf{R}_{i+1} = \mathbf{I} + \sin\theta_i\hat{\boldsymbol{\xi}} + \hat{\boldsymbol{\xi}}^2(1 - \cos\theta_i) \tag{11}$$

With local displacement $\mathbf{p}_{i,i+1}$ and ${}^i\mathbf{R}_{i+1}$ known, the global displacement of $\sum C_i$ can be obtained recursively

$$\mathbf{p}_i = \mathbf{p}_{i-1} + \mathbf{p}_{i-1,i} \quad (12)$$

$$\mathbf{R}_i = {}^{i-1}\mathbf{R}_i\mathbf{R}_{i-1} \quad (13)$$

with the initial displacement of $\mathbf{p}_1 = \mathbf{0}$ and $\mathbf{R}_1 = \mathbf{I}$.

4.3 Workspace Analysis

The workspace of the new ECM is defined by all the points that the manipulator tip can reach in 3D space. Based on the measurement of prototype, $R = 25\text{mm}$, range of d is from 42mm to 62mm, and $e = 2.3\text{mm}$. The workspace of the new ECM is generated accordingly and shown in Fig. 7.

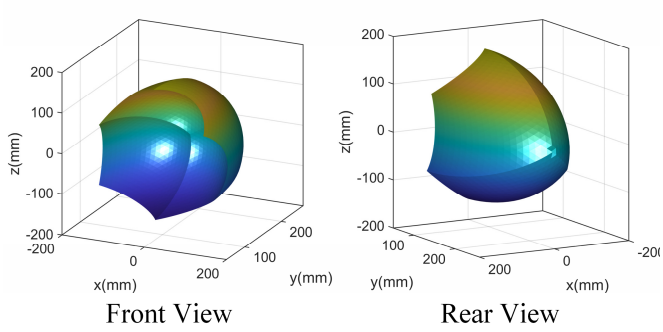

Figure 7. Workspace of the new ECM

The workspace shows that the fully shortened manipulator has a length of 176mm and the fully extended case has a length of 256mm. The maximal extension ratio (for what percentage the ECM can extend the most) is (256-176)/176=45.45%. The three ridges appearing on both the concave and the convex surfaces correspond to a single actuator driving cases.

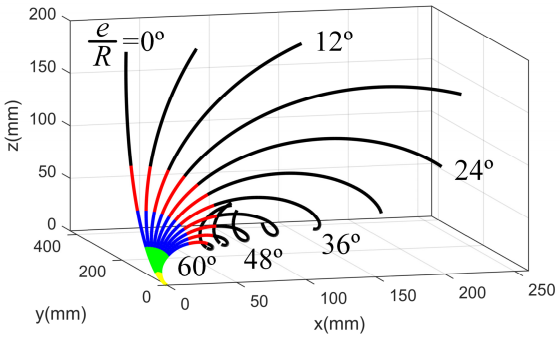

Figure 8. Twist effect for different e/R values

4.4 Motion Non-uniformity Evaluation

As discussed in section 3.1, due to the rod mounting angle shift $e/R \neq 0$, the "Measuring PM" cannot exactly copy the "Driving PM" motion. This fact leads to a twist motion along the manipulator axial direction, which breaks the desired uniform motion for each subsegment. To evaluate the non-uniformity induced by this phenomenon, different angle shift e/R values are tested and the corresponding manipulator configurations with the same inputs ($d_{1,1} = 42\text{mm}$, $d_{1,2} = 52\text{mm}$, $d_{1,3} = 52\text{mm}$) are plotted in Fig. 8., in which five more subsegments (in black) are added to make the twist motion more visible. The other colors indicate the four subsegments in the actual design.

As shown in Fig. 8, the twist effect becomes quite serious as e/R is beyond 10 degrees and more subsegments worsen the situation significantly. Therefore, for practical design purposes, reducing e to a value as small as possible and choosing fewer subsegments helps reducing the undesired twist motion. For the existing design with a minimized e value (2.3mm), the twist effect is also evaluated for different manipulator configurations. The non-uniformity is defined by the difference between the last subsegment bending plane angle φ_4 and the first subsegment bending plane angle φ_1. Numerical calculation is conducted and plotted in Fig. 9, which surprisingly shows that the non-uniformity (the value in the figure is 15.81°) is actually not affected by the manipulator configuration.

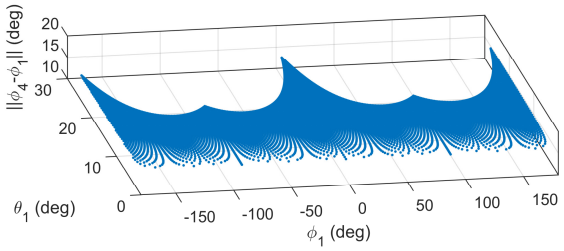

Figure 9. Distribution of non-uniformity for different ECM configurations

This can be verified analytically by substituting Eq. (8) into Eq. (6), which yields

$$-\tan(\varphi_{i+1} - \frac{e}{2R}) = \frac{m_{i,3} + m_{i,2} - 2m_{i,1}}{\sqrt{3}(m_{i,3} - m_{i,2})} \quad (14)$$

Substituting Eq. (7) into Eq. (14) and evaluating, Eq. (14) is simplified as

$$\varphi_{i+1} - \varphi_i = \frac{e}{R} \quad (15)$$

which means that the twist effect only depends on the rod mounting angle shift e/R and the subsegment number.

5 PROTOTYPING AND EXPERIMENTS

To verify the proposed mobility of the new mechanism, a proof-of-concept prototype was integrated with 3D printing (using ABS plastic as the building material). Three Actuonix linear actuators (L12-30-210-6-P) with corresponding controller boards were used to drive the manipulator. For the rack and pinion transmission, off-the-shelf 0.5 modulus nylon gears were utilized and customized racks were 3D printed. The flexible rods were made out of Trik Fish line with 1.35mm diameter. The rods and the plastic parts were connected by super glue.

As shown in Fig. 10, the prototype exhibits the proposed 2R1T mobility, for which the most shortened length is measured as 177mm and the most extended length as 234mm. The extension ratio is computed as 32.2% which is smaller than

the ratio predicted by the workspace analysis. This is partially due to the smaller range applied on the linear actuator to avoid potential damage on the prototype. The maximal bending angle was measured to be around 80 degrees.

Although the prototype demonstrates good bending shapes as a whole, the first subsegment was observed to have larger bending angles than the rest. The reason was partially due to the non-uniform motion effect that was discussed in section 3.1. But more importantly, the non-uniformity for the first subsegment comes from its large driving force. As shown above, the new manipulator mechanism utilizes the propagation way to transmit motion from the base to the link tip. From conservation of energy, we know that this method will accumulate and amplify the driving force from each subsegment onto the first subsegment, which makes its flexible rods to deform more than that of the rest. This observation suggests that a more accurate statics-based kinematic model is required to better calculate the manipulator shape.

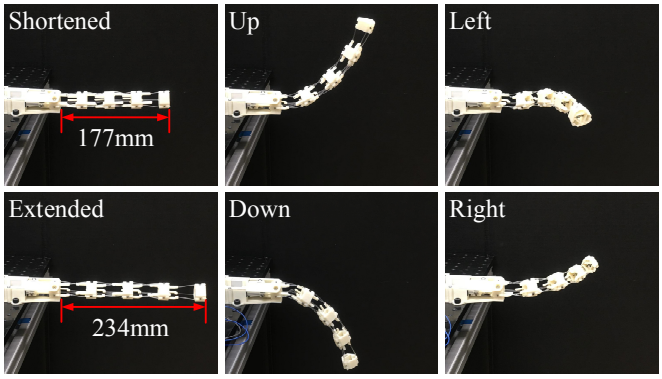

Figure 10. The new ECM mobility demonstration

6 CONCLUSION AND FUTURE WORK

By leveraging the rigid coupling hybrid mechanism concept and the flexible parallel mechanisms, a new 3DOF extensible continuum manipulator with spatial bending (2R) and one axial extension (1T) mobility was proposed. The core idea lies in using the motion of the *i*-th link to drive the (*i*+1)-th link so that the local motion can be copied and propagated from the base link to the tip link. To achieve this design goal, flexible parallel mechanism was used to realize the basic 2R1T subsegment motion and rack and pinion set was used to couple the adjacent subsegments. This way, the 2R1T motion is copied by each subsegment and the entire manipulator achieves spatial bending and one extension mobility. To calculate the configuration of this new mechanism, a simplified kinematic model was formulated. Workspace analysis was also carried out to evaluate the mechanism's capability. A small proof-of-concept was manufactured to verify the proposed mobility. Preliminary tests showed that for the current design, the new manipulator is able to extend 32% of its original length and bend over 80 degrees.

However, the kinematic model in this paper provided just a rough estimation of the actual shape, which ignores the static effects as well as the actual deformation shape of the rods (which can be more approximated by a spline instead of an arc). The first deficiency mainly causes the shape non-uniformity among subsegments since forces couple all parts in a static balancing system. The second deficiency mainly contributes to the shape error inside the subsegment, i.e. the subsegment wise kinematics. Therefore, one of the most important aspects of future work is to develop more accurate kinematic model based on the Coserrat rod theory, which will take the gravity, friction, and external loads into account. Moreover, improving the mechanical design to reduce the friction (e.g., using metal gear-rack sets with smaller modulus) will also be the focus. Considering the potential of this new manipulator for medical applications (e.g., minimally invasive surgery), and further miniaturizing the design is also an important pending future work.

ACKNOWLEDGMENTS

This material is partially based upon work supported by the National Science Foundation under Grant No. 1906727.

REFERENCES

[1] Hannan, M.W., and Walker, I.D., 2003, "Kinematics and the Implementation of an Elephant's Trunk Manipulator and Other Continuum Style Robots," Journal of robotic systems, 20(2), pp. 45-63.

[2] Li, C., and Rahn, C.D., 2002, "Design of Continuous Backbone, Cable-driven Robots," J. Mech. Des., 124(2), pp. 265-271.

[3] Simaan, N., Taylor, R. and Flint, P., 2004, April. A dexterous system for laryngeal surgery. IEEE International Conference on Robotics and Automation, New Orleans, LA, USA, USA, April 26-May 1, 2004, pp. 351-357.

[4] Chirikjian, G.S., and Burdick, J.W., 1995, "Kinematically Optimal Hyper-redundant Manipulator Configurations," IEEE transactions on Robotics and Automation, 11(6), pp. 794-806.

[5] Wright, C., Johnson, A., Peck, A., McCord, Z., Naaktgeboren, A., Gianfortoni, P., Gonzalez-Rivero, M., Hatton, R., and Choset, H., 2007, "Design of a Modular Snake Robot," IEEE/RSJ International Conference on Intelligent Robots and Systems, San Diego, CA, USA, October 29-November 2, 2007, pp. 2609-2614.

[6] Racioppo, P., and Ben-Tzvi, P., 2019, "Design and Control of a Cable-Driven Articulated Modular Snake Robot," IEEE/ASME Transactions on Mechatronics, 24(3), pp. 893-901.

[7] Liu, Y., Wang, J., and Ben-Tzvi, P., 2019, "A Cable Length Invariant Robotic Tail Using a Circular Shape Universal Joint Mechanism," Journal of Mechanisms and Robotics, 11(5), p. 051005.

[8] Rone, W.S., Saab, W., and Ben-Tzvi, P., 2018, "Design, Modeling, and Integration of a Flexible Universal Spatial Robotic Tail," Journal of Mechanisms and Robotics, 10(4), p. 041001.

[9] Saab, W., Rone, W.S., Kumar, A., and Ben-Tzvi, P., 2019, "Design and Integration of a Novel Spatial Articulated Robotic Tail," IEEE/ASME Transactions on Mechatronics, 24(2), pp. 434-446.
[10] Mehling, J.S., Diftler, M.A., Chu, M., and Valvo, M., 2006, "A Minimally Invasive Tendril Robot for In-space Inspection," The First IEEE/RAS-EMBS International Conference on Biomedical Robotics and Biomechatronics, Pisa, Italy, February 20-22, 2006, pp. 690-695.
[11] Nguyen, T.D., and Burgner-Kahrs, J., 2015, "A Tendon-driven Continuum Robot with Extensible Sections," IEEE/RSJ International Conference on Intelligent Robots and Systems, Hamburg, Germany, September 28-October 2, 2015, pp. 2130-2135.
[12] Zhang, K., Qiu, C., and Dai, J.S., 2016, "An Extensible Continuum Robot with Integrated Origami Parallel Modules," Journal of Mechanisms and Robotics, 8(3), p. 031010.
[13] Webster III, R.J., Romano, J.M., and Cowan, N.J., 2008, "Mechanics of Precurved-tube Continuum Robots," IEEE Transactions on Robotics, 25(1), pp. 67-78.
[14] Jones, B.A., and Walker, I.D., 2006, "Kinematics for Multisection Continuum Robots," IEEE Transactions on Robotics, 22(1), pp. 43-55.
[15] Liu, Y., and Ben-Tzvi, P., 2020, "Design, Analysis, and Integration of a New Two-Degree-of-Freedom Articulated Multi-Link Robotic Tail Mechanism," Journal of Mechanisms and Robotics, 12(2), p. 021101.
[16] Tanev, T.K., 2000, "Kinematics of a Hybrid (Parallel-Serial) Robot Manipulator," Mechanism and Machine Theory, 35(9), pp.1183-1196.
[17] Fan, C., Liu, H., and Zhang, Y., 2013, "Type Synthesis of 2T2R, 1T2R and 2R Parallel Mechanisms," Mechanism and Machine Theory, 61, pp.184-190.
[18] Li, Q., and Hervé, J.M., 2010, "1T2R Parallel Mechanisms Without Parasitic Motion," IEEE Transactions on Robotics, 26(3), pp. 401-410.
[19] Gogu, G., 2005, "Mobility of Mechanisms: a Critical Review," Mechanism and Machine Theory, 40(9), pp. 1068-1097.
[20] Wang, X., and Mills, J.K., 2006, "Dynamic Modeling of a Flexible-link Planar Parallel Platform Using a Substructuring Approach," Mechanism and Machine Theory, 41(6), pp. 671-687.
[21] Black, C.B., Till, J., and Rucker, D.C., 2017, "Parallel Continuum Robots: Modeling, Analysis, and Actuation-based Force Sensing," IEEE Transactions on Robotics, 34(1), pp. 29-47.
[22] Webster III, R.J., and Jones, B.A., 2010, "Design and Kinematic Modeling of Constant Curvature Continuum Robots: A Review. The International Journal of Robotics Research, 29(13), pp. 1661-1683.
[23] Kurdila, A.J., and Ben-Tzvi, P., 2019, Dynamics and Control of Robotic Systems, John Wiley & Sons, Hoboken, New Jersey.